J Appl Electrochem (2010) 40:701–708
DOI 10.1007/s10800-009-0047-4

ORIGINAL PAPER

An attempt to produce $NiFe_2O_4$ powder from electrodeposited Fe–Ni alloy powders by subsequent recrystallization in air

U. Lačnjevac · B. M. Jović · V. M. Maksimović · V. D. Jović

Received: 14 August 2009 / Accepted: 1 December 2009 / Published online: 18 December 2009

Abstract The electrodeposition of the Fe–Ni powders from citrate-ammonium chloride containing electrolytes for different Ni/Fe ions concentration ratios at pH 4.0 was investigated by the polarization measurements. The morphology, chemical composition, and phase composition of the obtained powders were investigated using SEM, EDS, and XRD analysis. EDS analysis of as-deposited alloy powders confirmed anomalous co-deposition of Fe and Ni. A common characteristic for all as-deposited powder samples was the presence of cone-shaped cavities and nodules on the big agglomerates of the order of 200–400 μm. After annealing in air at 400, 600, and 700 °C for 3 h, all alloy powders oxidized forming NiO, $NiFe_2O_4$, and Fe_2O_3 phases in different proportions depending on the original powder composition. The $NiFe_2O_4$ phase was found to be dominant in the sample with the highest percentage of Fe after annealing at 600 °C.

Keywords Fe–Ni · Powder · Electrodeposition · Morphology · Composition analysis · Recrystallization

1 Introduction

One of the components of the Fe–Ni system, formed by oxidation of Fe–Ni mixture at high temperatures, is a nickel ferrite, $NiFe_2O_4$, an inverse spinel in which the tetrahedral sites (A) are occupied by Fe^{3+} ions and octahedral sites (B) by Fe^{3+} and Ni^{2+} ions [1].

According to the literature [2, 3], the $NiFe_2O_4$ is the most suitable material for device applications in the upper microwave and lower millimeter wave ranges. At the same time, $NiFe_2O_4$ was found to be a highly reproducible humidity [4] and gas [5, 6] sensor material. The numerous techniques, such as ferrite plating [7, 8], oxidation of metallic films [9], arc plasma method [10], chemical transport [11, 12], chemica1 vapor deposition [13–16], the dip coating process [17], spray pyrolysis [18, 19], and pulsed wire discharge [20] have been used for preparation of the $NiFe_2O_4$ films. The main difficulty of these methods is the limit in the choice of substrate material, since it must be kept at a high temperature after deposition. Sartale et al. [21] has proposed less expensive and more popular method for the preparation of the spinel nanocrystalline $NiFe_2O_4$ films, based on the electrodeposition of $NiFe_2$ alloy coating from a non-aqueous ethylene glycol sulfate bath followed by electrochemical oxidation of the alloy in an aqueous bath at room temperature. It is shown that the air annealing of the as-deposited $NiFe_2O_4$ thin films at 500 °C for 5 h improves the crystallinity and morphology of the films. In the study of Fang et al. [22], the $NiFe_2O_4$ ultrafine powder with high crystallinity has been prepared through a reverse microemulsion route. After optimizing the composition in the starting solution, the resulting $NiFe_2O_4$ was formed at temperature of around 550–600 °C, which is much lower than that observed from the solid-state reaction. Magnetic investigation indicates that samples are soft-magnetic materials with low coercivity and with the saturation magnetization close to the bulk value of nickel ferrite. Most recently, $NiFe_2O_4$ nanoparticles were synthesized via solid-state reaction process of the $Fe_{67}Ni_{33}$ alloy nanopowder at different annealing temperatures in the air [23].

U. Lačnjevac · B. M. Jović · V. D. Jović (✉)
Institute for Multidisciplinary Research, University of Belgrade, P.O. Box 33, 11030 Belgrade, Serbia
e-mail: vladajovic@imsi.rs

V. M. Maksimović
Institute of Nuclear Sciences Vinča, P.O. Box 522, 11001 Belgrade, Serbia

It was shown by XRD and TEM analysis that $NiFe_2O_4$ started to form at around 450 °C, being well defined after annealing at 550 °C with the powder particle size ranging between 15 and 50 nm.

Most of the investigations concerning Fe–Ni alloys electrodeposition are in connection with the deposition of compact coatings [24–27], while the electrodeposition of Fe–Ni alloy powders was the subject of only few articles. Zhelibo et al. [28, 29] suggested a method for producing very fine Fe–Ni alloy powder by the electrolysis in a two-layer electrolytic bath using a hydrocarbon solvent from an oil refining fraction as an upper organic layer with evaporation at 180 °C and subsequent reduction annealing in a hydrogen atmosphere. The influence of the reduction annealing temperature [28] and the electrolysis temperature [29] on the formation, chemical and phase composition, structure, and magnetic properties of highly dispersed Fe–Ni alloy powders were investigated, and the optimal thermal conditions for the production of powders with micron-sized particles were determined [28, 29]. The effect of complexing agents (citric and oxalic acid) on the process of Fe–Ni alloy powders was also investigated [30]. It was shown that complexing agents influence the kinetics of powders of electrodeposition, as well as the morphology of the Fe–Ni powders. Finer powders were produced in the presence of citric acid in comparison with those obtained in the presence of oxalic acid [30]. Detailed analysis of the processes of Fe–Ni alloy powders electrodeposition from citrate-ammonium chloride and citrate-sodium sulfate containing electrolytes in the presence of Fe(III) and/or Fe(II) salts are presented in our previous article [31].

So far, electrochemical deposition of Fe–Ni powder with subsequent oxidation at high temperature in air has not been reported as a process for production of the nickel ferrite. In this study, an attempt was made to produce nickel ferrite powder from the electrodeposited Fe–Ni powders by subsequent annealing (recrystallization) in air.

2 Experimental

All powders were electrodeposited at the room temperature in the cylindrical glass cell (total volume of 1 dm^3) with cone-shaped bottom of the cell to collect powder particles. Fe–Ni alloy powders were deposited under galvanostatic conditions on glassy carbon cylinder ($d = 0.5$ cm, $h = 3$ cm) at the current density of 2.5 A cm^{-2} (see Sect. 3). All powders were washed with distilled water and alcohol after deposition and dried in air at 80 °C. Annealing of all powders was performed in air, first at the temperature of 400 °C for 3 h. After SEM, EDS, and XRD analysis powders were annealed at 600 °C for 3 h and analyzed by SEM, EDS, and XRD. Finally, since it was found that big powder agglomerates were not completely oxidized during annealing at 600 °C (see Sect. 3), powders were ground in mortar, annealed at 700 °C for 3 h, and analyzed by XRD.

All solutions were made from analytical grade purity chemicals ($NiCl_2$, $Na_3C_6H_5O_7$, NH_4Cl, $FeCl_2$) and distilled water.

The morphology of the electrodeposited powders was examined using scanning electron microscope (SEM), Tescan VEGA TS 5130MM equipped with an energy-dispersive X-ray spectroscopy (EDS), and INCAPentaFET-x3 detector, Oxford Instruments. Accordingly, composition of as-deposited and recrystallized powders was determined by the EDS analysis.

The phase composition of the as-deposited and recrystallized powders was investigated using a PHILIPS PW 1050 X-ray powder diffractometer.

Each experiment was repeated three times, and the average values are presented in this article. The variation of the results was ±5%.

3 Results and discussion

Four different electrolytes, with total metal ion concentration of 0.1 M, were used for the alloy powders electrodeposition: x M $NiCl_2$ + 1 M NH_4Cl + 0.2 M $Na_3C_6H_5O_7$ + y M $FeCl_2$: ($x = 0.09$, 0.075, 0.05 and 0.025 M and $y = 0.075$, 0.05, 0.025, and 0.01 M). In such a way, the Ni/Fe ion concentration ratios were 9/1, 3/1, 1/1, and 1/3, while the pH of the solution was kept constant (pH 4.0) by adding HCl. All powders for microstructure, composition, and phase composition analysis were electrodeposited practically at the limiting current density (position of the j_{pd} on the polarization diagrams, see Fig. 1b of [31]).

The polarization curves recorded in different electrolytes possess a similar shape. They are characterized by two inflection points, the first one reflecting massive alloy deposition (sharp increase of current density), and the second one (●) corresponding to the moment when the deposition process is controlled by the rate of hydrogen bubble formation, actually the potential at which the diffusion limiting current of alloy powder deposition is reached (as explained in our previous articles [32, 33]). The characteristics of the polarization diagrams for Ni–Fe powders electrodeposition are explained in great detail in our previous article [31].

The current efficiency for Fe–Ni powders electrodeposition has been determined by the procedure explained in great details in our previous articles [31–33]. It was found that the current efficiency varies from about 15% at low content of Fe in the powder, to about 8% at high content of Fe in the powder (see Fig. 2 of [31]), which is in

accordance with the statement [24] that the current efficiency for Fe–Ni alloy deposition decreases with the increase of Fe ions concentration in the electrolytes, i.e., with the increase of Fe content in the coating.

3.1 The morphology of the as-deposited powders

The main characteristic of the morphology of the Fe–Ni alloy powder particles electrodeposited onto glassy carbon electrode from different electrolytes is the presence of big agglomerates, shown in Fig. 1a. Their size was found to vary from about 200 to about 500 μm. The surface of these agglomerates is covered with nodules (Fig. 1b) and big and small cone-shaped cavities (Fig. 1c). The observed cavities correspond to the places where the hydrogen bubbles were formed [31–34]. Particularly interesting are crystals of the shape of pagoda present in the powder with about 70 at.% of Ni (Ni/Fe = 9/1) (see Fig. 9 of [31]). Such crystals were detected in the Fe–Ni powder synthesized in high yield by a simple and facile hydrothermal method without the presence of surfactants [35]. According to this investigation [35] $FeNi_3$ crystals were formed during the described procedure.

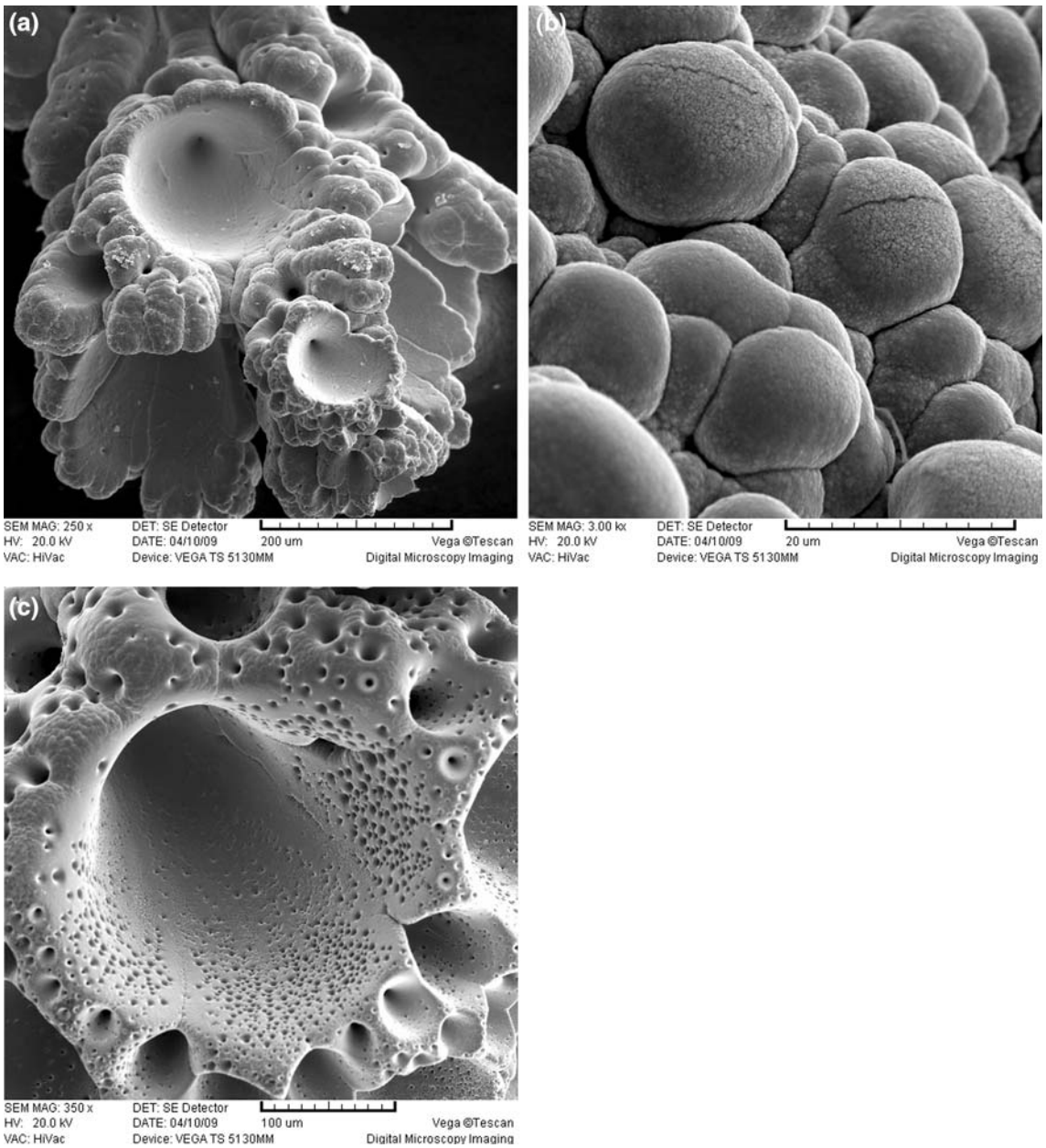

Fig. 1 Typical powder particles for all as-deposited Fe–Ni powders. All powders were deposited at the current density of 2.5 A cm^{-2}

The products obtained at 120 °C are mixture of $FeNi_3$ and Fe–Ni hydroxides composed of monodispersed microspheres. With the increase of temperature to 140 °C these microspheres become micropagodas very similar to those shown in Fig. 9 of [31]. At higher temperatures (180 °C), these particles transform into perfect 3D $FeNi_3$ dendritic superstructures in certain directions [35]. Hence, on comparison of the crystals presented in Fig. 9 of [31] with those obtained by hydrothermal method [35], it seems reasonable to ascribe them to the $FeNi_3$ single crystals (there is also an indication for the existence of $FeNi_3$ single crystals in as-deposited powder, see XRD analysis presented in Fig. 2). It should be noted here that at a given current density of deposition, further transformation into dendrites most likely could not be possible since the powder particles fall off from the electrode surface before the formation of dendrites.

3.2 The EDS analysis of the as-deposited powders

All powder samples were analyzed by EDS in such a way that at least eight powder particles (maximum number 11) on the SEM micrographs were chosen, and EDS analysis was performed at 3–10 different positions on each particle. In some cases, the analysis was performed at a point of 1 μm^2, while in some cases, rectangular surface from 120 μm^2 (10 × 12 μm) to 9,600 μm^2 (80 × 120 μm) has been analyzed. Hence, for the further analysis, the average values of composition for each analyzed particle were used. Since in all powder samples, oxygen was detected up to maximum 15 at.%, its content was subtracted assuming that only Fe and Ni are present in the powders (oxygen was probably from the remaining of the electrolyte and washing procedure and possibly due to limited oxidation during the drying procedure). In order to determine the type of Fe–Ni alloy powder deposition, the percentages of Fe and Ni determined by the EDS analysis were used, and results were presented in Fig. 10 of our previous study [31]. According to Brenner's classification [36], anomalous co-deposition of Fe and Ni occurs at all investigated solution compositions, with the less noble metal (Fe) being more readily deposited than the more noble one (Ni), i.e., the percentage of Ni in the powder is lower than its percentage in the solution.

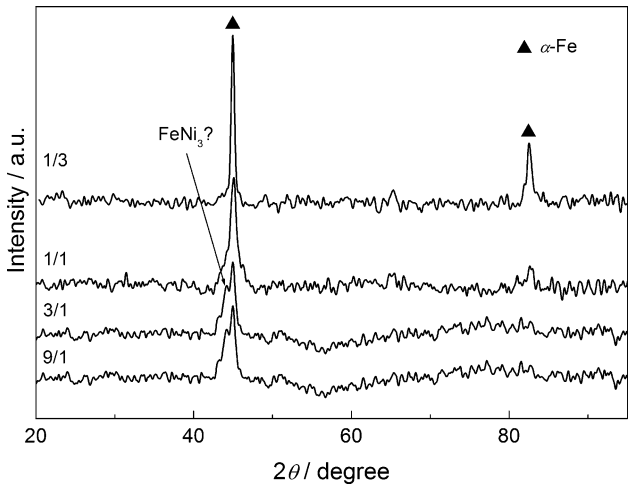

Fig. 2 XRD analysis for the as-deposited powders obtained from the solutions with different Ni/Fe ratios (marked in the figure: *filled triangle*) peaks of the α-Fe phase

3.3 The XRD analysis of the as-deposited powders

The diffractograms of the as-deposited powders are presented in Fig. 2. Because of very small crystallites size, ranging between 7 and 20 nm from Ni/Fe = 9/1 to Ni/Fe = 1/3 (determined from the half with of the peaks appearing on the diffractograms) only phases with the highest intensity were detected. Two peaks marked with (▲) best correspond to the α-Fe phase. Taking into account that the peaks for FeNi (kamacite) (37-0474), α-Fe (06-0696) and Ni (45-1027) practically overlap, broader peak at around 44.5° for Ni/Fe ratios 9/1, 3/1, and 1/1 could be ascribed to any of these phases. The appearance of a small peak at around 44.3 for Ni/Fe ratios 9/1 and 3/1 (marked with arrow in Fig. 2) could be an indication for the existence of $FeNi_3$ {111} (38-0419), taking into account the pagoda-like morphology detected on the surface of the agglomerates of these powders [31, 35].

3.4 The SEM, EDS, and XRD analysis of the recrystallized powders

During the first annealing procedure, powder samples were kept for 3 h at 400 °C in the furnace under the air atmosphere. Typical morphologies of the surface of annealed (recrystallized) powders particles (EDS) for all the investigated electrolyte compositions are shown in Fig. 3. The appearance of different type of crystals on powder particles surface for different Ni/Fe ions ratios is characteristic for these powders, as shown in Fig. 3a–d. In order to find out what is the composition of the obtained crystals the EDS analysis of all the samples is performed, and the results at different spectrum positions are given in Table 1. A common characteristic of the EDS analysis is the decrease of Ni content on the surface of analyzed samples with the decrease of Ni/Fe ratio (42 at.% Ni for the 9/1 ratio and 27 at.% Ni for the 3/1 ratio), i.e., the decrease of Ni content in the alloy powders, while for the Ni/Fe ratios 1/1 and 1/3 content of Ni on the powder particles surfaces is practically zero. It is interesting to note that on the surface of samples with the Ni/Fe ratios 1/1 and 1/3 some parts of the surface have been peeled off (Fig. 3c, d) and that the composition of the surface layer is completely different from that of the

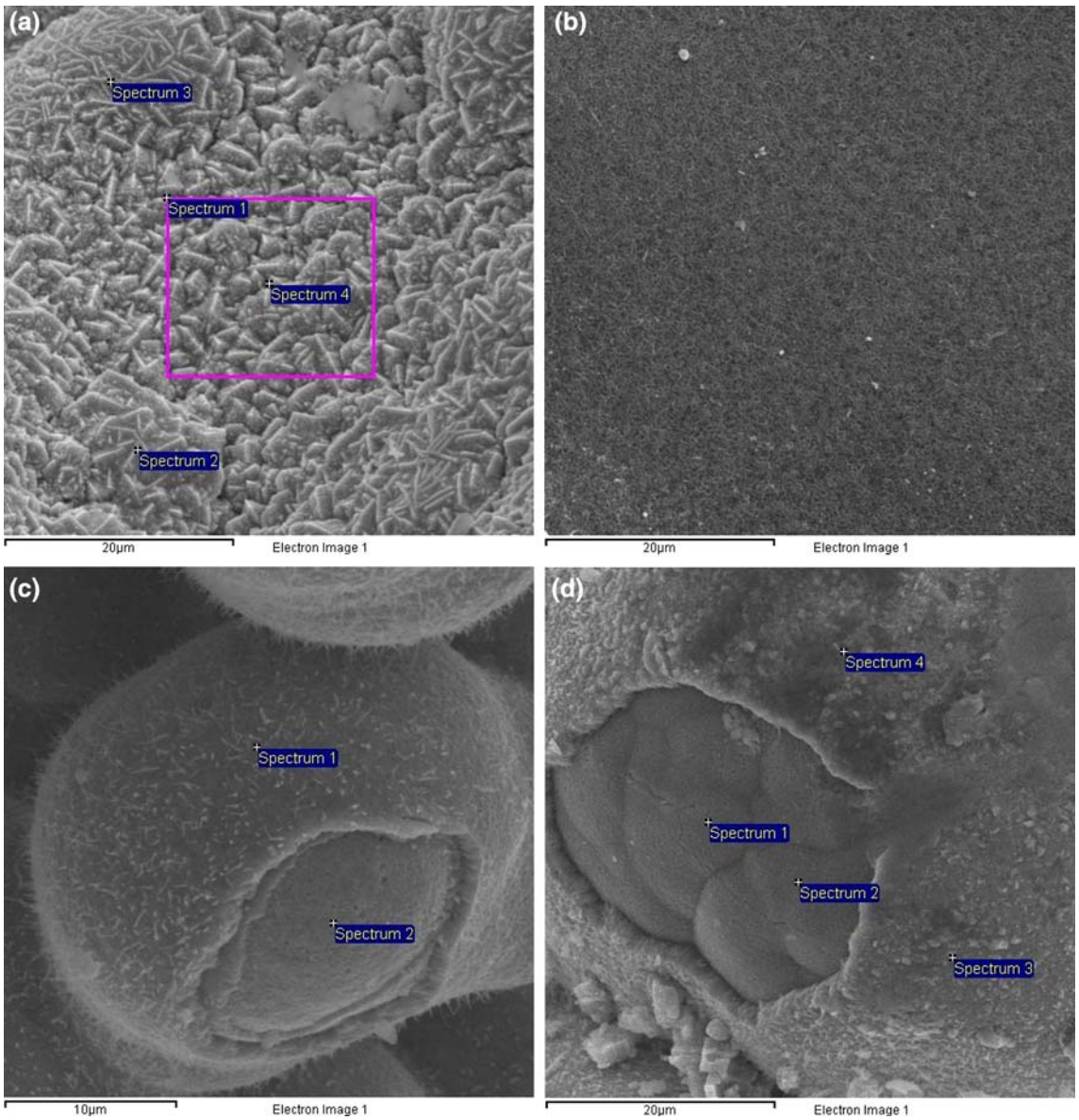

Fig. 3 The images with marked positions of the EDS spectra of the powder particles annealed at 400 °C for 3 h in the air atmosphere for powders electrodeposited at Ni/Fe = 9/1 (**a**), Ni/Fe = 3/1 (**b**), Ni/Fe = 1/1 (**c**), and Ni/Fe = 1/3 (**d**). Corresponding results of the EDS analysis are presented in Table 1

bulk of particle (Table 1). According to the EDS analysis of these two samples, it appears that the surface layer is composed of iron oxide (most likely Fe_2O_3), since the content of Ni is zero. For powder samples with lower content of Fe (Ni/Fe = 9/1 and 3/1, Fig. 3a, b), layered structure has not been observed (no peeling off of the surface layer has been detected), and accordingly, only the composition of the surface has been analyzed. Taking into account that for such surfaces EDS results cannot be considered as quantitative, a convincing conclusion about the properties of these powder particles surfaces could not be made. Hence, it appears from the EDS analysis of the powder particles surfaces that for samples with higher content of Fe (Ni/Fe = 1/1 and 1/3, Fig. 3c, d), the oxidation of all powders particles is not complete and that only surfaces are completely oxidized due to iron oxide diffusion to the surface of the particles during the oxidation process. Taking into account the dimensions of the powder particles (agglomerates, up to about 400 µm), it is quite possible that the oxidation process took place mostly on the particles surface. It is possible that the same conclusion could be valid for samples rich in Ni, but on the SEM micrographs peeling of the surface layer has not been detected.

During the second annealing procedure (additional annealing at 600 °C for 3 h in air), all the powder samples

Table 1 Results of the EDS analysis of powder samples electrodeposited from different electrolytes, obtained at different positions (spectra) at powder particles presented in Fig. 5

Ni/Fe	Spectrum number	at.% O	at.% Fe	at.% Ni
9/1	1	39	25	36
	2	24	23	53
	3	31	19	50
	4	41	29	30
3/1	1	57	19	24
1/1	1	48	52	0
	2	42	35	23
1/3	1	29	67	4
	2	51	43	6
	3	58	42	0
	4	51	49	0

were characterized with the presence of needle-like crystals on the surface of particles (most likely corresponding to the Fe_2O_3 phase), with their dimension being bigger for samples with higher content of Fe. This is shown in Fig. 4a for Ni/Fe ratios 9/1 and 3/1 and in Fig. 4b for Ni/Fe ratios 1/1 and 1/3. In comparison with the samples annealed at 400 °C, the EDS analysis showed higher content of Fe and O for samples obtained at Ni/Fe ratios 9/1 and 3/1, while for samples obtained at Ni/Fe ratios 1/1 and 1/3, identical results were obtained as those for the annealing at 400 °C.

In order to provide complete oxidation of powders, all the samples were ground in mortar, annealed at 700 °C for 3 h, and analyzed by XRD.

XRD results recorded after annealing at 400, 600, and 700 °C are shown in Fig. 5. These results are in good agreement with the EDS analysis, showing that all powder particles were oxidized during annealing, forming NiO, Fe_2O_3, and $NiFe_2O_4$ phases. As can be seen, the intensity of some peaks increases, while the intensity of some peaks decreases with increasing annealing temperature.

The intensity of Ni peak (■) was found to decrease with increasing annealing temperature for Ni/Fe ratios 9/1, 3/1, and 1/1, with Ni being most likely oxidized into NiO and/or $NiFe_2O_4$ phases. This phase practically disappeared in powders electrodeposited at the Ni/Fe ratio 1/3 annealed at all the temperatures. Its presence on the diffractograms recorded for the annealing temperatures 400 and 600 °C in powders electrodeposited at Ni/Fe ratios 9/1, 3/1, and 1/1 indicate that in these powders, Ni cannot be completely oxidized at given annealing temperatures. The disappearance of this phase in powder electrodeposited at Ni/Fe = 1/1 after annealing at 700 °C confirms that during additional oxidation whole amount of Ni has been oxidized.

The intensity of the peak for NiO phase (↓) increased with increasing annealing temperature for samples rich in Ni (Ni/Fe = 9/1 and 3/1), while for other two samples NiO peaks (↓) of small intensities were detected. As can be seen in Fig. 5, this phase practically disappeared in the powder electrodeposited at Ni/Fe ratio 1/3 after annealing at 700 °C.

The intensity of the peak for Fe_2O_3 phase (▼) also increased with increasing annealing temperature in all the samples. In samples with high content of Ni, this phase has not been detected on the diffractograms recorded after annealing at 400 °C only. After annealing at 700 °C, this phase became dominant in Fe-rich samples (Ni/Fe = 1/1 and 1/3).

Similar conclusion could be made for the $NiFe_2O_4$ phase (∇). In all the samples, peaks of this phase could be detected on the diffractograms recorded after annealing at 600 and 700 °C. It is interesting to note that the peaks of $NiFe_2O_4$ phase (∇) possess the highest intensity in the powder electrodeposited at Ni/Fe ratio 1/3 after annealing

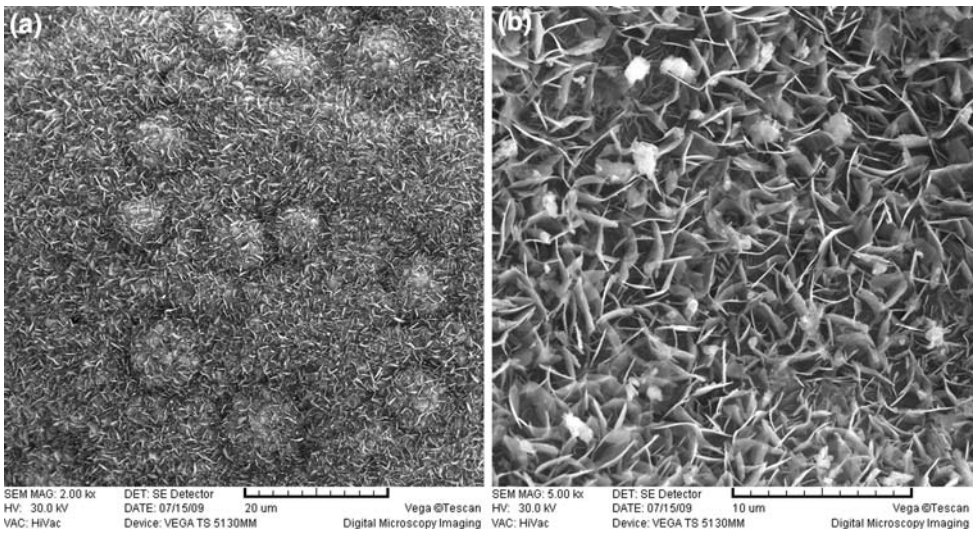

Fig. 4 The surfaces of powder particles after additional annealing at 600 °C for 3 h in the air atmosphere for powders electrodeposited at Ni/Fe = 9/1 and Ni/Fe = 3/1 (**a**) and Ni/Fe = 1/1 and Ni/Fe = 1/3 (**b**)

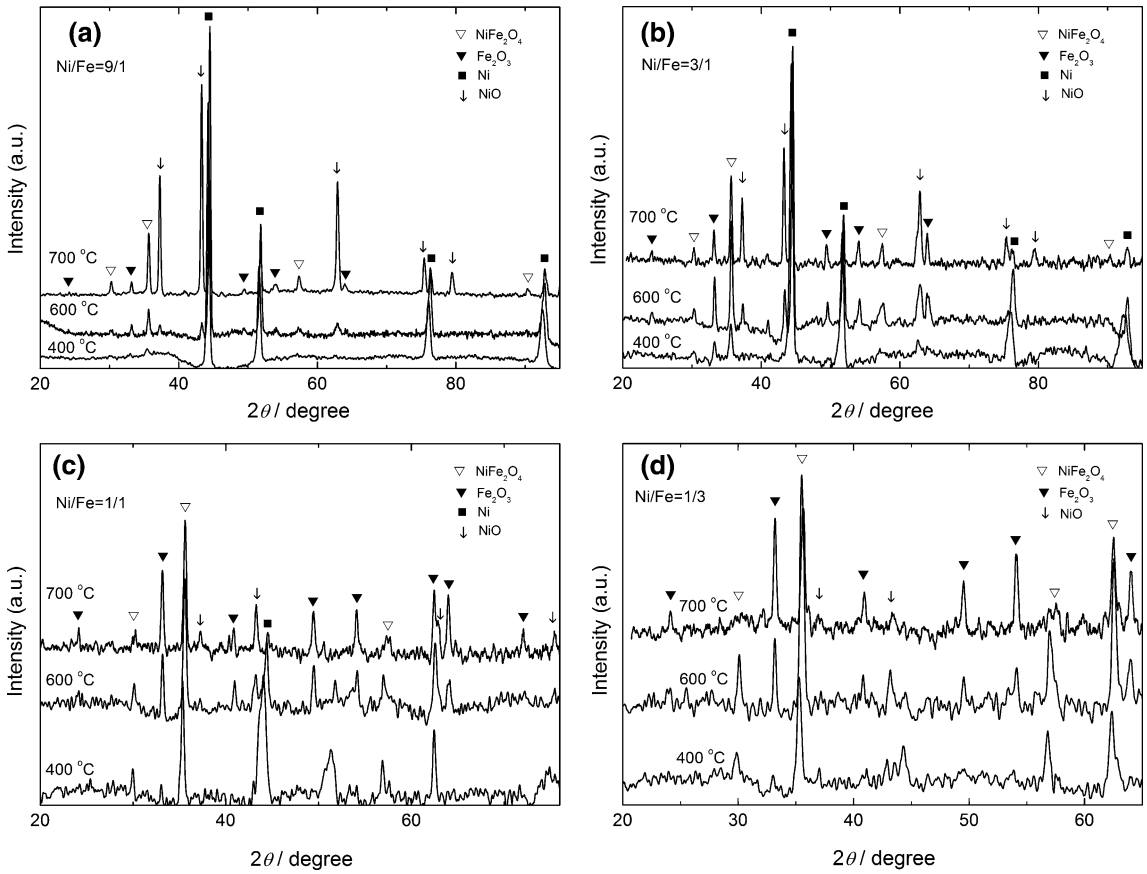

Fig. 5 XRD analysis for the powders annealed at 400, 600, and 700 °C (marked in the figure) obtained from the solutions with different Ni/Fe ratios: **a** Ni/Fe = 9/1; **b** Ni/Fe = 3/1; **c** Ni/Fe = 1/1; and **d** Ni/Fe = 1/3 (marked in the figure): peaks of the Ni phase (*filled square*); peaks of the NiO phase (*down arrow*); peaks of the $NiFe_2O_4$ phase (*open inverted triangle*); and peaks of the Fe_2O_3 phase (*filled inverted triangle*)

at 600 °C indicating that these are the best conditions for its formation. Such behavior is in accordance with the findings of Ceylan et al. [23] that well-defined $NiFe_2O_4$ nanoparticles crystallize at 550 °C after solid-state reaction in $Fe_{67}Ni_{33}$ nanopowder. Hence, it appears that for a powder composition 89 at.%. Fe–11 at.% Ni (powder obtained for Ni/Fe ratio 1/3), which is different from that for $Fe_{67}Ni_{33}$, dominant phase is $NiFe_2O_4$ after annealing of as-deposited powder at 600 °C.

4 Conclusions

The morphology and composition of as-deposited, as well as recrystallized alloy powders depend on the Ni/Fe ions concentration ratio. Anomalous co-deposition of Fe and Ni has been confirmed by the EDS analysis of as-deposited alloy powders. A common characteristic for all as-deposited powder samples was the presence of cone-shaped cavities and nodules. After annealing in air at 400, 600, and 700 °C for 3 h all the alloy powders oxidized forming NiO, $NiFe_2O_4$, and Fe_2O_3 with the NiO phase disappearing in the samples with higher percentage of Fe. The $NiFe_2O_4$ phase was found to be dominant in the sample with the highest percentage of Fe annealed at 600 °C. From the EDS and XRD analyses, it could be concluded that the powders were not completely oxidized during annealing in air at 400 and 600 °C.

Acknowledgments This study was financially supported by the Ministry of Science and Technological Development of the Republic of Serbia through the Project No. 142032G/2006.

References

1. Morrish AH, Haneda KJ (1981) Appl Phys 52:2496
2. Ishino K, Narumiya Y (1987) Am Ceram Soc Bull 66:1469
3. Zhang Q, Itoh T, Abe M, Tamaura Y (1992) In: Yamaguchi T, Abe M (eds) Ferrites Proceedings ICF-6, Tokyo, p 481
4. Dube GR, Darshane YS (1993) J Mol Catal 79:285
5. Reddy GCV, Manorama SV, Rao YJ (1999) Sens Actuators B 55:90
6. Satyanarayana LK, Reddy KM, Manorama SV (2003) Mater Chem Phys 82:21
7. Abe M, Itoh T, Tamaura Y et al (1998) J Appl Phys 63:3774
8. Itoh T, Abe M, Sasao T et al (1989) IEEE Trans Magn 25:4230

9. Suran G, Heurtel A (1972) J Appl Phys 43:536
10. Naoe M, Yamanaka S (1970) Jpn J Appl Phys 9:293
11. Marshall DJ (1971) J Cryst Growth 9:305
12. Gibart P, Robbins M, Kane AB (1974) J Cryst Growth 24–25:166
13. Pulliam GR (1967) J Appl Phys 38:1120
14. Mee JE, Pulliam GR, Archer JL et al (1969) IEEE Trans Magn 5:717
15. Fitzgerald AG, Engin R (1974) Thin Solid Films 20:317
16. Itoh H, Takeda T, Naka S (1986) J Mater Sci 21:3677
17. Tsuchiya T, Yamashiro H, Sei T et al (1992) J Mater Sci 27:3645
18. Jung DS, Kang YC (2009) J Magn Magn Mater 321:619
19. Deschanres JL, Langlet M, Joubert JC (1990) J Magn Magn Mater 83:437
20. Lee PY, Ishizaka K, Suematsu H et al (2006) J Nanocryst Res 8:29
21. Sartale SD, Lokhande CD, Giersig M et al (2004) J Phys Condens Matter 16:773
22. Fang J, Shama N, Tung L et al (2003) J Appl Phys 93:7483
23. Ceylan A, Ozcan S, Ni C et al (2008) J Magn Magn Mater 320:857
24. Kieling VC (1997) Surf Coat Technol 96:135
25. Yin K-M, Lin B-T (1996) Surf Coat Technol 78:205
26. Kim S-H, Sohn K-J, Joo Y-C et al (2005) Surf Coat Technol 199:43
27. Bento FR, Mascaro LH (2006) Surf Coat Technol 201:1752
28. Zhelibo EP, Kravets NN, MYu Gamarkin et al (1995) Powder Metall Metal Ceram 34:113
29. Zhelibo EP, Kravets NN (1997) Powder Metall Metal Ceram 36:264
30. Chu C-M (2003) J Chin Inst Eng 34:689
31. Lačnjevac U, Jović BM, Jović VD (2009) Electrochim Acta 55:535
32. Jović VD, Jović BM, Pavlović MG (2006) Electrochim Acta 51:5468
33. Jović VD, Jović BM, Maksimović V et al (2007) Electrochim Acta 52:4254
34. Jović VD, Maksimović V, Pavlović MG et al (2006) J Solid State Electrochem 10:373
35. Zhou X-M, Wei X-W (2009) Cryst Growth Des 9:7
36. Brenner A (1963) Electrodeposition of alloys: principles and practice. Academic Press Inc, New York and London